

DRAFT

Measuring the Magnetic Field on the Classical T Tauri Star TW Hydrae

Hao Yang

*Department of Physics & Astronomy, Rice University, 6100 Main St. MS-108, Houston,
TX 77005*

haoyang@rice.edu

Christopher M. Johns-Krull^{1,2}

*Department of Physics & Astronomy, Rice University, 6100 Main St. MS-108, Houston,
TX 77005*

cmj@rice.edu

Jeff A. Valenti¹

Space Telescope Science Institute, 3700 San Martin Dr., Baltimore, MD 21210

valenti@stsci.edu

ABSTRACT

We present infrared (IR) and optical echelle spectra of the Classical T Tauri star TW Hydrae. Using the optical data, we perform detailed spectrum synthesis to fit atomic and molecular absorption lines and determine key stellar parameters: $T_{\text{eff}} = 4126 \pm 24$ K, $\log g = 4.84 \pm 0.16$, $[M/H] = -0.10 \pm 0.12$, $v \sin i = 5.8 \pm 0.6$ km s⁻¹. The IR spectrum is used to look for Zeeman broadening of photospheric absorption lines. We fit four Zeeman sensitive Ti I lines near 2.2 microns and find the average value of the magnetic field over the entire surface is $\bar{B} = 2.61 \pm 0.23$ kG. In addition, several nearby magnetically insensitive CO lines show no excess broadening above that produced by stellar rotation and instrumental broadening,

¹Visiting Astronomer, Infrared Telescope Facility, operated for NASA by the University of Hawaii

²Visiting Astronomer, McDonald Observatory, operated by The University of Texas at Austin

reinforcing the magnetic interpretation for the width of the Ti I lines. We carry out extensive tests to quantify systematic errors in our analysis technique which may result from inaccurate knowledge of the effective temperature or gravity, finding that reasonable errors in these quantities produce a $\sim 10\%$ uncertainty in the mean field measurement.

Subject headings: infrared: stars — stars: magnetic fields — stars: pre-main sequence — stars: individual (TW Hya)

1. Introduction

T Tauri stars (TTs) are newly formed low-mass stars that have recently become visible at optical wavelengths. They are young, roughly solar mass stars, still contracting along pre-main sequence evolutionary tracks in the H-R diagram. TTs can be placed into two categories, depending on whether or not they are actively accreting. Classical T Tauri stars (CTTs) are still surrounded by disks of material that are undergoing accretion onto the central star, producing excess emission in the form of both lines and continuum at ultraviolet (UV), optical, infrared (IR), and radio wavelengths. Naked T Tauri stars (NTTs) are those TTs that do not appear to have close dusty accretion disks surrounding the central stars and show no indications of accretion onto the star¹. The properties of TTs have been reviewed by Appenzeller & Mundt (1989), Bertout (1989), Basri & Bertout (1993), and Ménard & Bertout (1999). It is within the disks surrounding CTTs that planetary systems form. Understanding the processes through which young stars interact with and eventually disperse their disks is critical for understanding the formation of planetary systems as well as understanding the rotational evolution of young stars.

Magnetic fields are believed to play a fundamental role throughout the star formation process, especially with regard to the interaction between a CTT and its circumstellar disk. Stellar magnetic fields are thought to truncate the disk near the corotation radius, directing the flow of accreting material toward the polar regions of the central star (Camenzind 1990, Königl 1991, Cameron & Campbell 1993, Shu et al. 1994, Paatz & Camenzind 1996). Stellar magnetic fields may also play a critical role in driving the strong winds/jets seen in

¹The term weak or weak-lined TTs (WTTs) is often used to refer to NTTs; however, WTTs is a designation based purely on the observed equivalent width of the H α emission line, and there are several examples of WTTs that are nevertheless accreting material from a circumstellar disk at rates comparable to that found for CTTs. Therefore, we will use NTTs to refer to stars which do not show any sign of accretion.

young stars. Therefore, a full understanding of the early evolution of young stars requires exploration of their magnetic field properties.

The most successful approach for measuring fields on late-type stars in general has been to measure Zeeman broadening of spectral lines in unpolarized light (e.g., Robinson 1980; Saar 1988; Valenti, Marcy, & Basri 1995; Johns–Krull & Valenti 1996). For any given Zeeman σ component, the wavelength shift caused by a magnetic field is

$$\Delta\lambda = \frac{e}{4\pi m_e c^2} \lambda^2 g B = 4.67 \times 10^{-7} \lambda^2 g B \quad \text{mÅ kG}^{-1}, \quad (1)$$

where g is the Landé- g factor of the transition, B is the strength of the magnetic field (in kG), and λ is the wavelength of the transition (in Å). The first direct detection of a magnetic field on a TTS was reported by Basri, Marcy, and Valenti (1992). These authors used the fact that moderately saturated magnetically sensitive lines will have an increase in their equivalent width in the presence of a magnetic field as the line components split to either side, increasing line opacity in the wings. Using this equivalent width technique, Basri et al. (1992) measured the field of the NTTS Tap 35, obtaining a value of the magnetic field strength, B , times the filling factor, f , of field regions of $Bf = 1.0 \pm 0.5$ kG. As the importance of magnetic fields on TTSs has become recognized, more effort has been put into their measurement. Guenther et al. (1999) used the same equivalent width technique to analyze spectra from 5 TTSs, claiming significant field detections for 2 stars.

Johns–Krull, Valenti, and Koresko (1999b - hereafter Paper I) have examined three (Königl 1991, Cameron & Campbell 1993, Shu et al. 1994) of the magnetospheric accretion theories and provide analytic expressions for the equatorial magnetic field strength at the surface of CTTSs. In the context of these theories, the surface field strength depends on the stellar mass, radius, rotation rate, and the mass accretion rate onto the star from the disk. In all these theories, a dipole field geometry is assumed. Paper I shows that the predicted dipole magnetic field strengths vary over a large range of values, including strengths up to several kilogauss. Such high field strengths should be directly measureable as Zeeman broadening in the line profiles of the most magnetically sensitive diagnostics.

Paper I made use of the wavelength dependence of the Zeeman effect (equation 1) to detect actual Zeeman broadening of a Ti I line at $2.2 \mu\text{m}$ on the CTTS BP Tau, measuring a field strength of $\bar{B} = 2.6 \pm 0.3$ kG, averaged over the entire surface. Johns–Krull, Valenti, and Saar (2004 - hereafter Paper II) analyzed 4 magnetically sensitive Ti I lines in K-band spectra of the NTTS Hubble 4, finding an average field strength of $\bar{B} = 2.5 \pm 0.2$ kG. Paper II also examined magnetically insensitive CO lines at $2.3 \mu\text{m}$ and detected no excess broadening above that due to rotation and instrumental broadening. Papers I and II also point out that the mean fields detected on BP Tau and Hubble 4 are larger than those

which can be confined by pressure balance with the quiet photosphere as discussed by Safer (1999); however, this is not a problem if the magnetic filling factor is unity in the visible photosphere. Indeed, the filling factor is unity in the dipole field configurations favored in current theoretical models (Königl 1991, Cameron & Campbell 1993, Shu et al. 1994).

Another method for detecting magnetic fields is to look for net circular polarization in Zeeman sensitive lines. Observed along a line parallel to the magnetic field, the Zeeman σ components are circularly polarized, with opposite helicity on either side of the nominal line wavelength. If the vector sum of magnetic fields on the stellar surface has a significant component along the line of sight, then net circular polarization becomes detectable. If the magnetic topology on the star is complex and small scale (as on the Sun), nearly equal amounts of both field polarities will generally be present producing negligible net polarization. Johns–Krull et al. (1999a) and Daou, Johns–Krull, and Valenti (2005) fail to detect polarization in photospheric absorption lines at 3σ upper limits of 200 G and 105 G respectively, seriously calling into question the assumed dipole field geometry. On the other hand, Johns–Krull et al. (1999a) discovered net polarization in the He I $\lambda 5876$ *emission* line on the CTTS BP Tau, indicating a net longitudinal magnetic field of 2.46 ± 0.12 kG in the line formation region. This He I emission line is believed to form in the post-shock region where disk material accretes onto the stellar surface (Hartmann, Hewett, & Calvet 1994; Edwards et al. 1994). Circular polarization in the He I line has now been observed in several CTTSs (Valenti & Johns–Krull 2004; Symington et al. 2005). These observations suggest that accretion onto CTTSs is indeed controlled by a strong stellar magnetic field.

While it is clear that at least a few TTSs possess kilogauss fields over most or all of their surfaces, it is also quite likely these fields are not dipolar. More observation of photospheric magnetic fields on TTSs are needed to test the assumptions and predictions of magnetospheric accretion theories. Here, we present an analysis of the photospheric magnetic field on the CTTS TW Hya, which is a K7Ve(Li) star (Herbig 1978) located at a distance of 56 ± 7 pc (Wichmann et al. 1998) in the TW Hydrae association. TW Hya is 13° from the nearest dark cloud, but it nonetheless has a disk with a mass of $\sim 5 \times 10^{-3} M_\odot$, as inferred from dust emission (Wilner et al. 2003). According to images at visible, near-IR, millimeter and sub-millimeter wavelengths (Krist et al. 2000; Wilner et al. 2000; Alencar & Batalha 2002; Weinberger et al. 2002; Qi et al. 2004), the optically thick disk is seen nearly face-on, extending to a radius of at least $3''.5$ (200 AU). Rucinski & Krautter (1983) find that TW Hya has all the properties of a classical T Tauri star, such as strong and variable Balmer emission lines (see also Webb et al. 1999) and a strong IR excess (see also Jayawardhana et al. 1999). Strong UV excess emission suggests ongoing accretion onto the star with an accretion rate estimated at $2 \times 10^{-9} M_\odot \text{yr}^{-1}$ (Herczeg et al. 2004). Age estimates for TW Hya range from 7 – 15 Myrs (Hoff et al. 1998, Webb et al. 1999, van Dishoeck et al. 2003).

Below, we report detection of Zeeman broadening in four Ti I lines in the K band, indicating that a strong magnetic field covers most or all of the surface of TW Hya. To further verify the magnetic nature of the detected broadening, several magnetically insensitive CO lines are also observed in the IR, exhibiting no broadening beyond that expected from stellar rotation as determined from an analysis of the optical spectrum. We also present an extensive analysis of possible systematic errors, finding that reasonable errors in effective temperature and gravity contribute only a $\sim 10\%$ uncertainty to the derived mean field. The observations and data reduction are described in § 2. In § 3 the analysis of the data is presented: § 3.1 examines the optical data used to determine the basic atmospheric parameters of TW Hya; while § 3.2 presents the analysis of the IR data to measure the magnetic properties of this star; and § 3.3 examines possible systematic errors in models used to analyze the IR data. A discussion of the results is given in § 4, and our conclusions are summarized in § 5.

2. Observations and Data Reduction

We obtained optical spectra at the 2.1 m Otto Struve telescope at McDonald Observatory on 1999 February 5 and 6. A Reticon 1200×400 CCD was used to record each spectrum covering the wavelength interval $5803 - 7376$ Å. The spectrograph slit was approximately $1''.07$ arcsec wide on the sky, which projected to ~ 2.14 pixels on the detector, resulting in a spectral resolving power of $R \equiv \lambda/\delta\lambda = 56,000$. These spectra were reduced using an automated echelle reduction package written in IDL that is described by Hinkle et al. (2000). Data reduction included bias subtraction, flat-fielding by a normalized incandescent lamp spectrum, scattered light subtraction, cosmic ray removal, and optimal extraction of the spectrum. Wavelengths were determined by fitting a two-dimensional polynomial to $n\lambda$ as function of pixel and order number, n , for several hundred thorium lines observed in an internal (part of the spectrograph assembly – post telescope) lamp. In addition to observations of TW Hya, spectra were also obtained of a rapidly rotating hot star, α Leo, at similar airmass to correct for contamination by telluric absorption lines. Table 1 summarizes the optical observations.

The K-band spectra presented here were obtained at the NASA Infrared Telescope Facility (IRTF) in April 1998. Observations were made with the CSHELL spectrometer (Tokunaga et al. 1990, Greene et al. 1993) using a $0''.5$ slit to achieve a spectral resolving power of $R \sim 36,200$, corresponding to a FWHM of ~ 2.7 pixels at the 256×256 InSb array detector. A continuously variable filter (CVF) isolated individual orders of the echelle grating, and a $0.0057 \mu\text{m}$ portion of the spectrum was recorded in each of 3 settings. The first two settings (2.2218 and $2.2291 \mu\text{m}$) each contain 2 magnetically sensitive Ti I lines. The

third setting ($2.3125\ \mu\text{m}$) contains several strong, magnetically insensitive CO lines. Each star was observed at two positions along the slit separated by $10''$. The K band spectra were reduced using custom IDL software described in Paper I. The reduction includes removal of the detector bias, dark current, and night sky emission. Flat-fielding, cosmic ray removal, and optimal extraction of the stellar spectrum are also included. Wavelength calibration for each setting is based on a 3rd order polynomial fitted to $n\lambda$ for several lamp emission lines observed by changing the CVF while keeping the grating position fixed. Dividing by the order number for each setting yields the actual wavelength scale for the setting in question. In each wavelength setting, we observed TW Hya and α Leo. The IR observations are also summarized in Table 1.

3. Analysis

The Ti I lines in the K band are excellent probes of magnetic fields on cool stars because of the λ^2 wavelength dependence of the Zeeman effect (equation 1) compared to the λ dependence of Doppler broadening. Here we measure the magnetic field on TW Hya by modeling the profiles of K band absorption lines. Since other line broadening mechanisms such as rotation are also potentially important, we must first demonstrate that we can accurately predict the appearance of the spectrum in the absence of a magnetic field. Several steps are required to achieve this goal, and the work here builds on the results of Papers I and II.

First, the optical spectrum of TW Hya is fit assuming no Zeeman broadening, since rotational and turbulent broadening dominate at these wavelengths. Based on fits to the solar spectrum in Paper I, we have precise atomic line data for the regions of the spectrum used here to determine atmospheric parameters. Fitting the optical spectrum of TW Hya yields the stellar parameters T_{eff} , $\log g$, $[\text{M}/\text{H}]$, $v \sin i$ and veiling (r). Using the resulting parameters, the nonmagnetic IR spectrum is predicted, and comparison with the observations shows obvious excess broadening in the observed Ti I line profiles, while no such excess broadening is seen in the magnetically insensitive CO lines. This excess width in the Ti I lines is then modeled as Zeeman broadening, using a polarized radiative transfer code. Matching the observed Ti I profiles then gives the strength and filling factor of magnetic regions on the surface of TW Hya.

3.1. Fit to the Optical Spectrum

The details of the spectrum synthesis and fitting procedure are given in Paper I. Briefly, spectra for the optical wavelength regions are calculated on a grid (in T_{eff} , $\log g$, and $[\text{M}/\text{H}]$) of model atmospheres. The nonlinear least squares technique of Marquardt (see Bevington & Robinson 1992) is used to fit the observed spectrum, solving for the key stellar parameters, namely, T_{eff} , $\log g$, $[\text{M}/\text{H}]$, $v \sin i$, and r . Spectra between model grid points are computed using three-dimensional linear (with respect to the model parameters T_{eff} , $\log g$ and $[\text{M}/\text{H}]$) interpolation of the resulting spectra. The model atmospheres are the “next generation” (NextGen) atmospheres of Allard & Hauschildt (1995). We interpolate the logarithm of the line depth rather than residual intensity, because the former quantity varies more slowly with changes in model parameters, yielding more accurate interpolated values. Rotational broadening is larger than the effects of macroturbulence in TW Hya, which makes it difficult to solve for v_{mac} . We adopt a fixed v_{mac} of 2 km s^{-1} from an extrapolation to K7 of class IV stars given in Gray (1992). It was found by Valenti et al. (1998) that in M dwarfs, microturbulence and macroturbulence were degenerate for the low turbulent velocities considered here. Therefore, microturbulence is neglected, allowing v_{mac} to be a proxy for all turbulent broadening in the photosphere. Spectra are synthesized in 3 optical regions, centered on 6151 \AA , 6498 \AA , and on the TiO bandhead at 7055 \AA , which provides excellent temperature sensitivity. Following Paper I, we only use features which are modeled well in both the solar spectrum and the spectrum of 61 Cyg B, a K7V reference star.

TW Hya model parameters determined by fitting the optical spectrum are given in the first row of Table 2. Observed and synthetic spectra for the three wavelength regions are shown in Figure 1. The Marquardt technique used to find the best fitting stellar parameters also gives formal uncertainties, but the actual uncertainties in derived parameters are completely dominated by systematic errors resulting from residual uncertainties in the line data and the model atmospheres used in the fit. To estimate these uncertainties we reanalyzed the observed spectra using 9 out of 10 atomic line intervals between $6140 - 6500 \text{ \AA}$ (indicated by contiguous bold segments in the bottom two panels of Figure 1), cycling through all 10 combinations. This procedure yields 10 alternate values for each model parameter and the standard deviation of each parameter value provides a more realistic estimate of its uncertainty. These uncertainties are listed in the second row of Table 2. The order containing the 7055 \AA molecular band head is always included in this procedure because this band head is such a strong temperature constraint. It is likely that our estimate of the systematic uncertainty on the T_{eff} determination is an underestimate.

3.2. Fits to the Infrared Data

Using the parameters (T_{eff} , $\log g$, $[M/H]$, and $v \sin i$) determined by the optical fits, we fit the magnetically insensitive CO lines at $2.3 \mu\text{m}$ and the magnetically sensitive Ti I lines at $2.2 \mu\text{m}$. The CO lines serve as a check that the parameters determined in the optical accurately represent the IR spectrum (particularly the line width), while the Ti I lines allow a determination of the magnetic field on TW Hya. The two categories of IR data are discussed separately below. Johns–Krull and Valenti (2001) find no K band veiling for this spectrum of TW Hya. Therefore, no veiling is used in the fits to the IR data for both the CO and Ti I line regions.

3.2.1. *Magnetically Insensitive CO Lines*

Line data for CO is taken from Goorvitch (1994) for the CO $X\Sigma^+$ state. We constructed a model atmosphere by interpolating a grid of NextGen model atmospheres to the T_{eff} , $\log g$, and $[M/H]$ obtained in the optical analysis. We then synthesized the CO line spectrum and convolved with a Gaussian corresponding to the spectral resolving power of the observed spectrum. Continuum normalization was the only free parameter used to match the observed and synthetic spectra, which are compared in Figure 2. The shape of the synthetic spectrum is determined entirely by parameters obtained in the optical analysis. Within the signal-to-noise ratio of the data, the model spectrum in Figure 2 shows good agreement with the observed spectrum, yielding a reduced χ^2 of $\chi_r^2 = 2.00$. Line strengths are off slightly, but this could in principle be corrected by tuning CO oscillator strengths. However, our primary concern is the widths of the CO lines, which are accurately reproduced by the synthetic spectrum, demonstrating that we are correctly modeling the dominant nonmagnetic broadening mechanisms.

3.2.2. *Magnetically Sensitive Ti I Lines*

Single Field Component Model

We start by applying a simple model in which some fraction of the surface is covered by a field of a single strength, while the rest of the surface is field free. Such a model is then specified by a single field strength, B , and the filling factor, f , of that field on the surface. By analogy to the mean field direction in solar plage, we assume a radial field geometry in the stellar photosphere. We assume that thermal structures are identical in magnetic and

field-free (quiet) regions. This is appropriate for optically thin flux tubes (e.g., plage), but probably not for large spots. The thermal structure of magnetic regions on TTS is unknown, nor are any applicable models available for use in our analysis.

The spectrum synthesis including magnetic fields has been described in Paper I. Only one Ti I line was used to model magnetic fields on BP Tau in Paper I. Strong K band veiling in BP Tau masked any line strength uncertainty due to errors in atomic data. In the case of Hubble 4 in Paper II, there is no K band veiling and all the Ti I lines used here were available to model. After comparing with the solar spectrum and that of 61 Cyg B, the gf values of the 4 Ti I lines were adjusted to match the profiles observed in 61 Cyg B. Here for TW Hya, we adopt the gf values for the Ti I lines from Paper II. The Marquardt technique is used again to solve for the best fitting values of the magnetic field strength and the filling factor. The key atmospheric parameters (T_{eff} , $\log g$, $[M/H]$, and $v \sin i$) are held fixed at values determined from the analysis of the optical data. The best fit to the IR data with a single field component model yields $B = 3.35$ kG and $f = 0.66$, and this model is shown in Figure 3 along with the model assuming no magnetic field on TW Hya. The model with a magnetic field is clearly a much better fit to the observed spectrum, yielding a reduced χ^2 of $\chi_r^2 = 1.70$ (computed considering only the points in the Ti I lines shown in bold in Figure 3). The non-magnetic model with all parameters fixed to values from the optical analysis gives $\chi_r^2 = 5.63$. For comparison with the models below, we note that $\bar{B} \equiv Bf = 2.21$ kG for this model.

Multi-Component Field Models

The single field component model provides a decent fit to the observed lines; however, the strengths of the lines at 2.22112 and 2.22740 μm are over-predicted. In addition, the observed profiles are broad and smooth, while the computed profiles show obvious inflection points. In Paper I this motivated the authors to construct multi-component field models which provided the best fit to BP Tau Ti I profile. In Paper II several multi-component field models are applied and improved the fits as well. It was also found in Paper I that multicomponent models with too many field components are degenerate since it is difficult to constrain separate field components with relatively small differences in field strength due to the combined effects of the spectrometer resolution and stellar rotation. In the case of BP Tau in Paper I, the effective magnetic resolution is about 2 kG. For Hubble 4 in Paper II, the high $v \sin i$ of 14 km s^{-1} lowers the resolution of Zeeman components, but simultaneous fitting of four Ti I lines with different Landé- g values improves the situation, resulting in approximately the same effective magnetic resolution as the analysis of BP Tau in Paper I. Here, in the case of TW Hya, the $v \sin i$ is only about 6 km s^{-1} . Following the calculations

in Paper II, an effective magnetic resolution of ~ 1.5 kG is estimated. Motivated by our previous results, we apply multi-component magnetic field models to TW Hya. We start with a two field component model to fit the data.

The two field component model divides the surface of the star into three regions: two covered with magnetic fields of different strengths and filling factors, and the last region is field-free. The sum of the filling factors of the three components must be 1.0, and the spectra from the different regions are multiplied by their filling factors and summed to generate the final model spectrum. We again use the Marquardt technique to find magnetic field strengths and filling factors that produce the best fit to the observed line profiles. The two field component model yields a somewhat smoother fit to the observed line profiles with a smaller χ_r^2 value of 1.29. The resulting magnetic field strengths and filling factors for the best fit are $B_1 = 3.0$ kG, $f_1 = 0.56$ and $B_2 = 6.5$ kG, $f_2 = 0.16$. The mean field on the stellar surface for this model is $\bar{B} = B_1 f_1 + B_2 f_2 = 2.72$ kG. To estimate uncertainties caused by potential errors in the atmospheric parameters derived from optical analysis, we re-analyze the IR spectra using a grid of assumed atmospheric parameters in which we vary $T_{\text{eff}} \pm 400$ K from the value in the default model, vary $\log g$ down by 0.5 from the default model, and vary [M/H] down by 0.5 from the default model. This results in a total of 12 different fits to the observed line profiles. Taking the mean and standard deviation of the resulting \bar{B} values gives a new estimate of $\bar{B} = 2.44 \pm 0.25$ kG on the stellar surface.

In order to explore whether additional components improve the fit significantly, we repeated the analysis described above for models with three or more components, each with a distinct field strength. For each model, we determined the filling factors for each component by fitting the observed Ti I line profiles, using the Marquardt algorithm. Table 3 summarizes our results for three different multi-component models: M1 includes components with field strengths of 0 – 5 kG in steps of 1 kG, M2 includes components with field strengths of 1 – 5 kG in steps of 2 kG, and M3 includes components with field strengths of 0 – 6 kG on steps of 2 kG. The last two rows of Table 3 give the reduced χ^2 and mean magnetic field over the surface for each model. All three models produce good fits to the data and indicate average field strength over the entire surface of 2.6 – 2.8 kG. Model M1 with 1 kG steps is underconstrained, given the Zeeman resolution of 1.5 kG discussed above, leading to an anomalously low filling factor for the 1 kG component, relative to the 0 and 2 kG components. Models M2 and M3 with 2 kG steps are well constrained. Given our Zeeman resolution, we cannot tell whether the component with the weakest field has a characteristic field strength of 0 kG or 1 kG.

Fig 4 compares model M3 with the observations. The reduced χ^2 for these models is similar to but slightly larger than that found from the two field component model, suggesting

that 2 components are adequate to fit the data for TW Hya. The differing values of \bar{B} derived from all the models considered reflect the systematic uncertainty associated with the choice of the model used to analyze the data. Since models M1, M2, and M3 and the two field component model have similar χ_r^2 values, we take the mean and standard deviation of these as our best estimate for the average field on TW Hya: $\bar{B} = 2.71 \pm 0.08$ kG. Above, we found that taking into account potential errors in the assumed stellar parameters resulted in an additional 10% uncertainty which we add in quadrature to that just given, to arrive at a final mean field estimate of $\bar{B} = 2.71 \pm 0.28$. Given that we have spent some considerable effort to derive accurate stellar parameters for TW Hya, we believe this is a conservative estimate of the uncertainty in the mean magnetic field.

3.3. Test of Analysis Technique

As described above, we determined the magnetic properties of TW Hya by fitting the IR spectra of Ti I lines in the K band. In this section, we use a Monte Carlo analysis to assess the stability of our analysis technique and the possible impact of systematic errors. We synthesize model spectra with a range of known magnetic properties, adding noise comparable to the uncertainty in our actual observations, and then we analyze each synthetic spectrum using our analysis technique. To create simulated observations, we adopted stellar parameters appropriate for a typical K7 TTS similar to TW Hya, namely $T_{\text{eff}} = 4000$ K, $\log g = 3.5$, $[\text{M}/\text{H}] = 0.0$, and $v \sin i = 6.0$ km s⁻¹.

We analyze each simulated observation 100 times with different realizations of the noise and random initial guesses for the magnetic field and its filling factor. In all cases we analyze the simulated data assuming the same nonmagnetic stellar parameters used to generate the artificial data. Results are shown in Table 4. The first two columns of the table give the input magnetic field strength and filling factor used to generate the simulated observation. The third column gives the number of good runs out of 100 trials. A bad run occurs when the program returns B values trapped in a local minimum between 10 – 20 kG due to noise in the data. Their χ_r^2 values are approximately twice those of the “good” fits, and plots of the fit show that they do not match the data. The fourth and fifth columns give average values of B and f for all good runs. The sixth and seventh columns give the ratio of \bar{B} to its input value and the corresponding standard deviation of this ratio. Errors in measured \bar{B} due to noise in the data are typically 5% or less, if T_{eff} , $\log g$, and $[\text{M}/\text{H}]$ are accurate.

Padgett (1996) found that in a sample of 30 TTSs the effective temperatures determined from spectral classification differ from the value obtained from measurements of line ratios in high resolution spectra. The absolute value of the difference averages 150 K with a scatter

up to 600 K. Additionally, gravities for TTSs usually come from placing stars in the H-R diagram using uncertain distances and then comparing with uncertain pre-main sequence evolutionary tracks. Although we determine T_{eff} and $\log g$ spectroscopically, our atmospheric parameters could still be subject to error. Thus, we use Monte Carlo tests to explore the effect of such errors on our derived magnetic parameters. Table 5 shows the results for a 200 K error in T_{eff} , while Table 6 shows the results for a 0.5 dex error in $\log g$. The Monte Carlo tests show that in the absence of accurate effective temperatures or gravities, the resulting systematic errors in the derived mean field is about 10% for typical field values and reasonable errors in temperature or gravity.

4. Discussion

Using high resolution optical spectra, we determine the key atmospheric parameters for TW Hya which are listed in Table 2. These values are generally in good agreement with previously published estimates. The calibration between spectral type and T_{eff} given by Cohen and Kuhn (1979) is often used in studies of TTSs. This calibration is essentially that of Johnson (1966), which is based on IR photometric studies of cool main sequence stars. For K7 spectral type, $T_{\text{eff}} = 4000$ K with a quoted 2% uncertainty. Bessel (1991) also derives $T_{\text{eff}} = 4000$ K for K7 stars by comparing broadband fluxes with blackbody distributions. We obtain an effective temperature of 4126 ± 24 K for TW Hya. From Papers I and II, BP Tau and Hubble 4 – both K7 stars – were found to have $T_{\text{eff}} = 4055 \pm 112$ K and $T_{\text{eff}} = 4158 \pm 56$ K, respectively. A statistical study of previous results for T_{eff} and spectral type for 268 stars by de Jager and Nieuwenhuijzen (1987) yields $T_{\text{eff}} = 4150 \pm 200$ K for K7 spectral type.

Previous results for the projected rotation velocity include $v \sin i = 4 \pm 3$ km s⁻¹ from Torres et al. (2000), $v \sin i < 6.0$ km s⁻¹ from Johns-Krull and Valenti (2001), and 5 ± 2 km s⁻¹ from Alencar and Batalha (2002). All agree well with our value of 5.8 ± 0.6 km s⁻¹. To our knowledge, there has been no previous determination of the metallicity of TW Hya. Our value of $[M/H] = -0.11 \pm 0.12$ is well within the range of $[Fe/H]$ values reported by Padgett (1996) in her study of several TTSs. For $\log g$, Alencar and Batalha (2002) obtain a value of 4.44 ± 0.05 using the line synthesis models of Barbuy (1982) and Valenti and Piskunov (1996). Our value of $\log g = 4.84 \pm 0.16$ is somewhat high, and differs from this estimate by 2.4σ . The sensitivity to gravity in our analysis comes from the depth of the TiO bandhead (which is also quite temperature sensitive) as well as from the two strong lines at 6493.8 Å and 6495.0 Å which show damping wings. We generally avoid more sensitive gravity diagnostics such as the Na I D lines since their profiles in CTTSs are usually contaminated by emission and/or absorption from circumstellar material. In the previous section, we show

that this difference of 0.40 in $\log g$ is expected to produce no more than a 10% error in our mean magnetic field estimate, which we account for in our quoted uncertainties.

TW Hya has a luminosity of $\log(L_*/L_\odot) = -0.62 \pm 0.11$, where the uncertainty in luminosity is dominated by uncertainty in the Hipparcos parallax. Combining this luminosity with our spectroscopically determined T_{eff} yields a stellar radius of $R_* = 0.96 \pm 0.12 R_\odot$. This radius together with our spectroscopic gravity estimate yields a mass of $M_* = 2.31 \pm 0.69 M_\odot$, where the uncertainty in our spectroscopic mass has roughly equal contributions from the uncertainties in $\log g$ and R_* . Comparing the location of TW Hya on an HR Diagram with pre-main sequence evolutionary tracks of D’Antona & Mazzitelli (1994) and Palla & Stalher (1999) yields stellar masses of $M_* = 0.79 M_\odot$ and $0.80 M_\odot$ respectively. Our spectroscopic mass is substantially larger than that estimated from evolutionary tracks and reflects our high value of $\log g$. Given the large uncertainty in our spectroscopic mass, the discrepancy is only 2.2σ . If we instead use the $\log g$ reported by Alencar and Batalha (2002), we find $M_* = 0.93 \pm 0.10$, in better agreement with evolutionary tracks.

Papers I and II determined spectroscopic and evolutionary track masses for BP Tau and Hubble 4. While the difference in any individual case is not statistically significant, it is interesting that in all three analyses to date, the spectroscopic masses are larger than masses based on evolutionary tracks. For stars with mass less than or equal to $1.2 M_\odot$, Hillenbrand and White (2004) found a similar trend in their study of stars with dynamically determined masses. The same result is also found by Reiners, Basri, and Mohanty (2005) in their analysis of a pre-main sequence double lined spectroscopic binary in Upper Scorpius. Therefore, it is likely that current pre-main sequence evolutionary tracks do indeed systematically underestimate the mass of young stars. For main-sequence stars, Valenti and Fischer (2005) find an analogous discrepancy between spectroscopic and isochrone masses, though the magnitude of the discrepancy is typically only 0.1 dex.

On the other hand, the mass we derive based on our gravity estimate is quite high relative to these evolutionary tracks. In order to explore the effect of this on our analysis, we use R_* determined above and M_* from evolutionary tracks to calculate $\log g = 4.38$. With this $\log g$, we reanalyze our optical spectra and obtain another set of atmospheric parameters: $T_{\text{eff}} = 4110$ K, $[M/H] = -0.23$, $v \sin i = 6.2 \text{ km s}^{-1}$, and $r = 0.61$. This fit returns a slightly larger χ_r^2 and is shown as the dash-dotted line in Figure 1. In addition, we fit the single magnetic component model with these atmospheric parameters and find $\bar{B} = 2.07$ kG. This fit returns $\chi_r^2 = 1.88$ and should be compared with our best fit single field component model with our previously determined atmospheric parameters which yields $\bar{B} = 2.21$ kG and $\chi_r^2 = 1.70$. The new atmospheric parameters produce a $\sim 6\%$ difference in the resulting mean field, confirming the results found above which showed that reasonable errors in the

assumed gravity produce $\sim 10\%$ or less error in the derived magnetic field properties.

In Paper I, Johns–Krull et al. examine the magnetospheric accretion models of Königl (1991), Cameron & Campbell (1993), and Shu et al. (1994) and summarize analytic equations for the predicted surface magnetic field strength of each model as a function of stellar mass, radius, rotation rate, and disk accretion rate. Using equations (2) – (4) of Paper I, and adopting an accretion rate of $\dot{M} = 2 \times 10^{-9} M_{\odot} \text{ yr}^{-1}$ from Herczeg et al. (2004), a rotation period $P = 2.2$ days from Mekkaden (1998), along with the stellar radius ($0.96 R_{\odot}$) and mass ($2.31 M_{\odot}$) estimated above, we estimate B_* . The Königl (1991) model gives $B_* = 2.78$ kG, while the Cameron & Campbell (1993) model gives $B_* = 0.60$ kG, and the model of Shu et al. (1994) predicts $B_* = 2.74$ kG. Our measured $\bar{B} = 2.71 \pm 0.28$ kG is very close to the predictions Königl (1991) and Shu et al. (1994), while it is larger than the prediction of Cameron and Campbell (1993). However, we caution that our measurement is just the unsigned field *strength*; we are unable to comment on the magnetic field geometry, which theories currently assume is dipolar.

Combining our measured average field strength with our calculated stellar radius, we can estimate the total stellar magnetic flux on the star. Pevtsov et al. (2003) find a nearly linear relationship between total unsigned magnetic flux and X-ray luminosity, L_X , for solar features (ranging from the smallest scales up to the entire Sun) and dwarf stars. Using this relationship, we predict $L_X = 1.41 \pm 0.14 \times 10^{30} \text{ erg s}^{-1}$. This value agrees well with the observed values of $0.90 - 1.76 \times 10^{30} \text{ erg s}^{-1}$ from Kastner et al. (2002) assuming a distance of 56 pc.

We can also use our magnetic field measurements to test the concept of pressure equipartition in the stellar photosphere. Spruit & Zweibel (1979) computed flux tube equilibrium models, showing that magnetic field strength is expected to scale with gas pressure in the surrounding non-magnetic photosphere. Field strengths set by pressure equipartition appear to be observed in G and K dwarfs (e.g. Saar 1990, 1994, 1996) and possibly in M dwarfs (e.g. Johns–Krull & Valenti 1996). Most TTSs have relatively low surface gravities and hence low photospheric gas pressures, so that equipartition flux tubes would have relatively low magnetic field strengths compared to cool dwarfs. Indeed, Safier (1999) examined in some detail the ability of TTS photospheres to confine magnetic flux tubes via pressure balance with the surrounding quiet photosphere, concluding that the maximum field strength allowable on TTSs is substantially below the current detections. On the other hand, it is doubtful that pressure equipartition arguments should hold when the magnetic field filling factor approaches unity on the stellar surface. Saar (1996) finds that the magnetic field strength does rise above the pressure equipartition value for very active K and M dwarfs once the filling factor reaches a value near one. Papers I and II found that the mean fields

on BP Tau and Hubble 4 are too large to be confined by gas pressure in the surrounding photosphere, suggesting that magnetic fields cover the entire surface.

TW Hya is an interesting case because its older age and corresponding higher surface gravity imply higher equipartition magnetic field strengths. Using the atmospheric parameters from Table 2, we find that the photospheric gas pressure in the atmosphere at the level where the local temperature is equal to the effective temperature implies a maximum field strength of 2.78 kG. Adopting the lower gravity of $\log g = 4.38$ and the associated temperature and metallicity described above gives a field strength of 2.14 kG at this same level in the stellar atmosphere. The first estimate is very similar to the derived mean field while the second is only somewhat lower. The two field component model and the multi-component models M1 - 3 all indicate that substantial portions of the stellar surface is covered by fields larger than these equipartition estimates; however, it is not certain that these observations demand unit filling factor of field regions in the case of TW Hya. In the analysis above, it was assumed that the atmospheric structure of the magnetic regions is identical to that in the non-magnetic regions (the magnetic regions are neither hot plage-like regions nor cool spot-like regions). In the Sun, the field strength in cool spots is a factor of ~ 2 larger than the typical value found outside of spots. As discussed in Paper II (see also Guenther et al. 1999), cool spot-like regions (and to a lesser extent hot plage-like regions) can affect the derived filling factor of these fields, but have a relatively weak effect on the derived field strength when actual Zeeman broadening is detected. The strong field regions on TW Hya are only about a factor of 2 stronger than the pressure equipartition field value, and the majority of the field found on TW Hya is near this equipartition value. Therefore, on TW Hya, the strong fields may be confined to cool spots while the weaker fields exist in plage-like regions on the surface of the star, and there is no need to assume unit filling factor of magnetic field regions.

Since TTSs generally are heavily spotted stars (e.g. Herbst et al. 1994 and references therein; Strassmeier, Welty, & Rice 1994 and references therein), there may be a need to model the observed spectra with 2 atmospheric components, each with a different effective temperature. In sunspots (and presumably starspots), magnetic pressure partially evacuates the spot, changing its density structure relative to the surrounding atmosphere. Unfortunately, there are no models for the atmospheric structure of spots on stars other than the Sun, and constructing such models is well beyond the scope of this paper. One could imagine trying to use model atmospheres simply scaled down in effective temperature (keeping the gravity and metallicity fixed) to begin to explore magnetic fields in spots and the resulting effect they might have on magnetic field analysis on TTSs. Paper II did just this for Hubble 4, finding that models with spots which were constrained to be 1000 K cooler than the non-spotted atmosphere had more difficulty simultaneously matching the optical and IR spectra

than did models without a spot contribution. The analysis of Hubble 4 also showed that the derived mean field from the spot model was within 18% of the derived mean field from the single component fit, with the change entirely due to the derived filling factor. While spots contribute relatively more to the continuum in the IR than in the optical, the strong temperature sensitivity of the TiO bandhead at 7055 Å results in significant contributions to this feature from spots and is a key constraint for any model. Building on these results, we restricted the modeling in this paper to a single effective temperature model. We note though that our predicted CO line strengths are fairly close to the observed line strengths, and that lowering the effective temperature by 300 K actually produces a slightly higher χ_r^2 for the CO line profiles. Evidently, the K band spectrum on TW Hya is not dominated by a substantially cooler (spot) component on the star.

Realistic models of spot atmospheres are needed to make further progress on testing just how much cool spots may contribute to the magnetic fields we have detected on TW Hya and other TTSs. In Paper II a spot model was used, but it was simply the atmosphere of a cooler star, with the same gravity and metallicity as that found for Hubble 4. On the Sun, magnetic pressure support partially evacuates the gas in a spot, changing its density compared to the quiet atmosphere. Such effects need to be considered for TTS (and other cool stars such as dMe stars). In addition, since it appears that strong magnetic fields on TTSs are also present in a substantial portion of the non-spotted photosphere, atmospheric models taking into account the magnetic pressure support should also be considered for this component of the atmosphere. Such a modeling effort is well beyond the scope of the current paper, but these results should be regarded as an appeal to theoreticians to begin to consider such problems, particularly since the data presented here clearly indicates the presence of strong magnetic fields on a large portion of TW Hya. Such strong fields have also been inferred for a handful of other TTSs (Basri et al. 1992, Guenther et al. 1999, Papers I and II), and these strong fields are likely to be a common feature of TTSs given their strong X-ray emission (e.g. Feigelson et al. 2003). Incorporating the effects of the magnetic field on the atmospheric structure will likely have important consequences beyond simply determining more accurate magnetic field parameters on TTSs. Perhaps it is the influence of these fields on the atmospheric structure that is responsible for the inconsistent mass determinations for TTSs described above? Future work is needed to know for sure.

5. Conclusion

We analyzed high resolution optical spectra of the classical T Tauri star TW Hya. We successfully fitted numerous atomic and molecular line features in 3 wavelength regions,

which are modeled well in both the solar spectrum and the spectrum of 61 Cyg B, a K7V reference star. In the process we determined the key atmospheric parameters (T_{eff} , $\log g$, $[\text{M}/\text{H}]$, $v \sin i$, and veiling) of the star.

With these atmospheric parameters, we simultaneously fit 4 magnetically sensitive Ti I lines at $2.2 \mu\text{m}$ to look for Zeeman broadening. We also fit several magnetically insensitive CO lines at $2.3 \mu\text{m}$ to verify that the parameters determined from optical analysis accurately reproduce the IR spectrum of TW Hya. The CO model spectrum agrees well with the data, and the fit to Ti I lines using various magnetic models yields a surface magnetic field strength of $\bar{B} = 2.71 \pm 0.28 \text{ kG}$, averaged over the entire surface of TW Hya.

We tested the sensitivity and stability of our analysis to systematic errors in the effective temperature and gravity, finding that errors of 200 K in T_{eff} or 0.5 dex in $\log g$ only result in a systematic error of $\sim 10\%$ in the derived mean magnetic field. Our measured field strength on TW Hya agrees well with the field strength expected from magnetospheric accretion models. However, we caution that these models assume a dipolar field geometry, and the data presented here do not constrain the field geometry on TW Hya. Circular polarization measurements, on the other hand, would provide strong constraints on the dipole field geometry of TW Hya.

CMJ-K and HY would like to acknowledge partial support from the NASA Origins of Solar Systems program through grant number NAG5-13103 made to Rice University.

REFERENCES

- Alencar, S. H. P. & Batalha, C. 2002, *ApJ*, 571, 378
- Allard, F. & Hauschildt, P. H. 1995, in *Bottom of the Main Sequence and Beyond*, ed. C.G. Tinney (Berlin: Springer), 32
- Appenzeller, I. & Mundt, R. 1989, *A&ARv*, 1, 291
- Barbuy, B. 1982, Ph.D. thesis, Université de Paris VII
- Basri, G. & Bertout, C. 1993, *Structure and Emission Properties of Accretion Disks*, *Proceedings of IAU Colloq.* 129, p. 189
- Basri, G., Marcy, G. W., & Valenti, J. A. 1992, *ApJ*, 390, 622
- Bertout, C. 1989, *ARARv*, 27, 351
- Bessel, M. S. 1991, *ApJ*, 101, 2
- Bevington, P. R. & Robinson, D. K. 1992, *Data Reduction and Error Analysis for the Physical Sciences*, (New York: McGraw Hill)
- Camenzind, M. 1990, *Rev. Modern Astron.*, (Berlin: Springer-Verlag), 3, 234
- Cameron, A. C. & Campbell, C. G. 1993, *A&A*, 274, 309
- Cohen, M. & Kuhi, L. V. 1979, *ApJS*, 41, 743
- D’Antona, F., & Mazzitelli, I. 1994, *ApJS*, 90, 467
- Daou, A. G., Johns-Krull, C. M. & Valenti, J. A. 2005, in preparation
- de Jager, C. & Nieuwenhuijzen, H. 1987, *A&A*, 177, 217
- Edwards, S., Strom, S. E., Hartigan, P., Strom, K. M., Hillenbrand, L. A., Herbst, W., Attridge, J., Merrill, K. M., Probst, R., & Gatley, I. 1993, *AJ*, 106, 372
- Goorvitch, D. 1994, *ApJS*, 95, 535
- Gray, D. F. 1992, *The Observation and Analysis of Stellar Photospheres*, (Cambridge: Cambridge Univ. Press)
- Greene, T. P., Tokunaga, A. T., Toomey, D. W., & Carr, J. B. 1993, *Proc. SPIE*, 1946, 313
- Guenther, E. W., Lehmann, H., Emerson, J. P., & Staude 1999, *A&A*, 341, 768
- Hartmann, L., Hewett, R., & Calvet, N. 1994, *ApJ*, 426, 669
- Hillenbrand, L. A. & White, R. J. 2004, *ApJ*, 604, 741
- Herbig, G. H. 1978, in *Problems of Physics and Evolution of the Universe*, ed. L. V. Mirzoyan, *Publ. Armenian Academy of Sci.*, Yerevan, p.171

- Herbst, W., Herbst, D. K., Grossman, E. J., & Weinstein, D. 1994, *AJ*, 108, 1906
- Herczeg, G. J., Wood, B. E., & Linsky, J. L., Johns–Krull, C. M. & Valenti, J. A. AAS, Meeting 205, #156.04
- Hinkle, K., Wallace, L., Valenti, J., & Harmer, D. 2000, Visible and Near Infrared Atlas of the Arcturus Spectrum 3727-9300 Å ed. K. Hinkle, L. Wallace, J. Valenti, & D. Harmer. (San Francisco: ASP) ISBN: 1-58381-037-4
- Hoff, W., Henning, T., & Pfau, W. 1998, *A&A*, 336, 242
- Jayawardhana, R., Hartmann, L., Fazio, G., Fisher, R. S., Telesco, C. M., Piña, R. K. 1999, *ApJ*, 521, 129
- Johnson, H. L. 1966, *ARA&A*, 4, 193
- Johns–Krull, C. M. & Valenti, J. A. 1996, *ApJ*, 459, L95
- Johns–Krull, C. M., Valenti, J. A., & Koresko, C. 1999b, *ApJ*, 516, 900 (Paper I)
- Johns–Krull, C. M., & Valenti, J. A. 2001, *ApJ*, 561, 1060
- Johns–Krull, C. M., Valenti, J. A., Saar, S. H. 2001, *ApJ*, 617, 1204
- Johns–Krull, C. M., Valenti, J. A., Hatzes, A. P., & Kanaan, A. 1999a, *ApJ*, 510, L41
- Kastner, J. H., Huenemoerder, D. P., Schulz, N. S., Canizares, C. R., Weintraub, D. A. 2002, *ApJ*, 567, 434
- Krist, J. E., Stapelfeldt, K. R., Ménard, F., Padgett, D. L., & Burrows, C. J. 2000, *ApJ*, 538, 793
- Königl, A. 1991, *ApJ*, 370, L39
- Ménard, F. & Bertout, C. 1999, *NATO ASIC Proc. 540: The Origin of Stars and Planetary Systems*, 341
- Mekkaden, M. V. 1998, *A&A*, 340, 135
- Nordström, B., Latham, D. W., Morse, J. A., Milone, A. A. E., Kurucz, R. L., Anderson, J., & Stefanik, R. P. 1994, *A&A*, 287, 338
- Paatz, G. & Camenzind, M. 1996, *A&A*, 308, 77
- Padgett, D. L. 1996, *ApJ*, 471, 847
- Palla, F. & Stahler, S. W. 1999, *ApJ*, 525, 772
- Pevtsov, A. A., Fisher, G. H., Acton, L. W., Longcope, D. W., Johns–Krull, C. M., Kankelborg, C. C., & Metcalf, T. R. 2003, *ApJ*, 598, 1387

- Qi, C., Ho, P. T. P., Wilner, D. J., Takakuwa, S., Hirano, N., Ohashi, N., Bourke, T. L., Zhang, Q., Blake, G. A., Hogerheijde, M., Saito, M., Choi, M., Yang, J. 2004, *ApJ*, 616, 11
- Reiners, A., Basri, G., & Mohanty, S. 2005, *ApJ*, in press
- Robinson, R. D. 1980, *ApJ*, 239, 961
- Rucinski, S. M. & Krautter, J. 1983, *A&A*, 121, 217
- Saar, S. H. 1988, *ApJ*, 324, 441
- Saar, S. H. 1990, *IAU Symp.* 138, *Solar Photosphere: Structure, Convection, and Magnetic Fields*, ed. J. O. Stenflo (Dordrecht: Kluwer), 427
- Saar, S. H. 1994, *IAU Symp.* 154, *Infrared Solar Physics*, eds. D. M. Rabin et al. (Dordrecht: Kluwer), 493
- Saar, S. H. 1996, *IAU Symp.* 176, *Stellar Surface Structure*, eds. K. G. Strassmeier & J. L. Linsky (Dordrecht: Kluwer), 237
- Safier, P. N. 1999, *ApJ*, 510, 127
- Shu, F. H., Najita, J., Ostriker, E., Wilkin, F., Ruden, S., & Lizano, S. 1994, *ApJ*, 429, 781
- Spruit, H. C., & Zweibel, E. G. 1979, *Sol. Phys.*, 62, 15
- Strassmeier, K. G., Welty, A. D., & Rice, J. B. 1994, *A&A*, 285, L17
- Symington, N. H., Harries, T. J., Kurosawa, R., & Naylor, T. 2005, *MNRAS*, 358, 977
- Tokunaga, A. T., Toomey, D. W., Carr, J. B., Hall, D. N. B., & Epps, H. W. 1990, *Proc. SPIE*, 1235, 131
- Torres, G., Guenther, E. W., Marschall, L. A., Neuhäuser, R., Latham, D. W., & Stefanik, R. P. 2003, *ApJ*, 125, 825
- Trilling, D. E., Koerner, D. W., Barnes, J. W., Ftaclas, C., Brown, R. H. 2001, *ApJ* 552, L151
- Valenti, J. A., & Fischer, D. A. 2005, *ApJS*, in press
- Valenti, J. A., & Johns-Krull, C. M. 2004, *Ap&SS*, 292, 619
- Valenti, J. A., Marcy, G. W., & Basri, G. 1995, *ApJ*, 439, 939
- Valenti, J. A., & Piskunov, N. 1996, *A&AS*, 118, 595
- Valenti, J. A., Piskunov, N., & Johns-Krull, C. M. 1998, *ApJ*, 498, 851
- van Dishoeck, E. F., Thi, W. F., & van Zadelhoff, G. J. 2003, *A&A*, 400, L1
- Webb, R. A., Zuckerman, B., Platais, I., Patience, J., White, R. J., Schwartz, M. J., & McCarthy, C. 1999, *ApJ*, 512, L63

- Weinberger, A. J., Becklin, E. E., Schneider, G., Chiang, E. I., Lowrance, P. J., Silverstone, M., Zuckerman, B., Hines, D. C., & Smith, B. A. 2002, *ApJ*, 566,409
- Wichmann, R. Bastian, U. Krautter, J. Jankovics, I., & Rucinski, S. M. 1998, *MNRAS*, 301L, 39
- Wilner, D. J., Bourke, T. L., Wright, C. M., Jørgensen, J. K., van Dishoeck, E. F., & Wong, T. 2003, *ApJ*, 596,597
- Wilner, D. J., Ho, P. T. P., Kastner, J. H., & Rodríguez, L. F. 2000, *ApJ*, 534,101

Table 1: Journal of observations.

Wavelength Setting	Main Lines	UT date	UT time	Observatory	Total exposure time(s)
2.2228 μm	Ti I	16-Apr-98	06:47	IRTF	3200
2.2300 μm	Ti I	14-Apr-98	07:39	IRTF	4500
2.31294 μm	CO	15-Apr-98	07:37	IRTF	6300
5803 – 7376 \AA	TiO	05-Apr-99	07:28	McDonald	10800
5803 – 7376 \AA	TiO	06-Apr-99	07:10	McDonald	7200

Table 2: Best fit atmospheric parameters for optical spectra.

	T_{eff}	$\log g$	$v \sin i$		
Param	(K)	(cm s ⁻²)	[M/H]	(km s ⁻¹)	Veiling
Value	4126	4.84	-0.11	5.80	0.61
σ	24	0.16	0.13	0.63	0.15

Table 3: Multi-component magnetic fits.

	M1	M2	M3
$f_{0\text{kG}}$	0.20	...	0.18
$f_{1\text{kG}}$	0.04	0.32	...
$f_{2\text{kG}}$	0.20	...	0.38
$f_{3\text{kG}}$	0.28	0.45	...
$f_{4\text{kG}}$	0.12	...	0.32
$f_{5\text{kG}}$	0.16	0.23	...
$f_{6\text{kG}}$	0.11
χ_r^2	1.32	1.34	1.31
\bar{B} (kG)	2.6	2.8	2.7

Table 4: Test results for fitting artificial data created assuming $T_{\text{eff}} = 4000$ K, $\log g = 3.5$, $[\text{M}/\text{H}] = 0$, and $v \sin i = 6.0 \text{ km s}^{-1}$. Artificial data is fit assuming the same atmospheric parameters as those used to create the data.

Model		good	Aver. of Results			
$B(G)$	f	runs	$B(G)$	f	Bf/Bf_{exp}	σ
1000	0.25	88	911.14	0.23	0.802	0.0549
1000	0.50	98	1001.6	0.52	1.032	0.0028
1000	0.75	97	931.08	0.80	0.988	0.0011
2000	0.25	100	1823.9	0.30	1.079	0.0051
2000	0.50	100	1866.3	0.52	0.977	0.0062
2000	0.75	100	2092.9	0.72	1.005	0.0004
3000	0.25	100	3005.3	0.23	0.917	0.0103
3000	0.50	100	3020.6	0.50	1.017	0.0008
3000	0.75	100	2975.7	0.75	0.996	0.0003
4000	0.25	98	4581.8	0.25	1.089	0.1532
4000	0.50	100	4185.4	0.51	1.051	0.0759
4000	0.75	99	4173.2	0.74	1.005	0.0920

Table 5: Test results for fitting artificial data created assuming $T_{\text{eff}} = 4000$ K, $\log g = 3.5$, $[\text{M}/\text{H}] = 0$, and $v \sin i = 6.0 \text{ km s}^{-1}$. Artificial data is fit assuming $T_{\text{eff}} = 4200$ K, $\log g = 3.5$, $[\text{M}/\text{H}] = 0$, and $v \sin i = 6.0 \text{ km s}^{-1}$.

Model		good	Aver. of Results			
$B(G)$	f	runs	$B(G)$	f	Bf/Bf_{exp}	σ
1000	0.25	98	493.81	0.97	1.840	0.1172
1000	0.50	97	747.11	0.98	1.461	0.0321
1000	0.75	100	962.16	0.96	1.185	0.1310
2000	0.25	100	1074.1	0.61	1.303	0.0047
2000	0.50	99	1568.4	0.75	1.181	0.0023
2000	0.75	100	1737.5	0.96	1.112	0.0255
3000	0.25	100	2335.1	0.32	0.982	0.0029
3000	0.50	100	2773.1	0.60	1.111	0.0005
3000	0.75	100	2790.3	0.92	1.138	0.0128
4000	0.25	100	3803.4	0.26	0.986	0.0006
4000	0.50	99	3818.8	0.56	1.073	0.0617
4000	0.75	100	3866.5	0.90	1.157	0.0070

Table 6: Test results for fitting artificial data created assuming $T_{\text{eff}} = 4200$ K, $\log g = 3.5$, $[\text{M}/\text{H}] = 0$, and $v \sin i = 6.0 \text{ km s}^{-1}$. Artificial data is fit assuming $T_{\text{eff}} = 4200$ K, $\log g = 4.0$, $[\text{M}/\text{H}] = 0$, and $v \sin i = 6.0 \text{ km s}^{-1}$.

Model		good	Aver. of Results			
$B(G)$	f	runs	$B(G)$	f	Bf/Bf_{exp}	σ
1000	0.25	89	7819.6	0.05	1.579	0.2942
1000	0.50	86	1660.9	0.19	0.629	0.0631
1000	0.75	100	1547.2	0.31	0.640	0.0380
2000	0.25	100	3580.8	0.16	1.011	0.1441
2000	0.50	100	2417.3	0.38	0.920	0.0004
2000	0.75	100	2180.9	0.61	0.888	0.0385
3000	0.25	98	4386.1	0.23	1.236	0.5194
3000	0.50	100	3279.8	0.48	1.030	0.1015
3000	0.75	100	3208.0	0.67	0.925	0.0554
4000	0.25	99	4635.2	0.24	1.113	0.2760
4000	0.50	99	4221.4	0.47	0.972	0.1333
4000	0.75	100	4164.3	0.69	0.930	0.1459

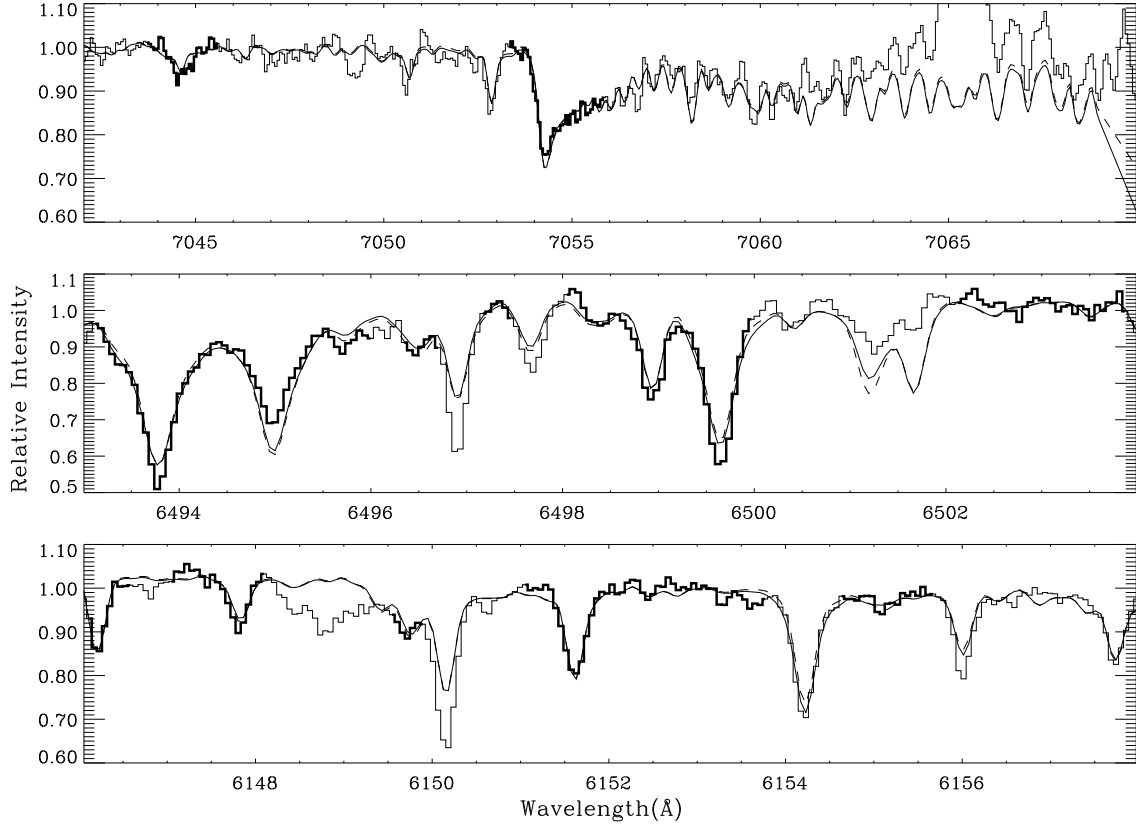


Fig. 1.— Best fit to the optical spectra (histogram : data ; smooth solid line : best fit with $\log g$ as a free parameter ; dash-dotted line : best fit with $\log g$ fixed at 4.38). The thick regions of the histogram are the spectral regions actually used in the fit.

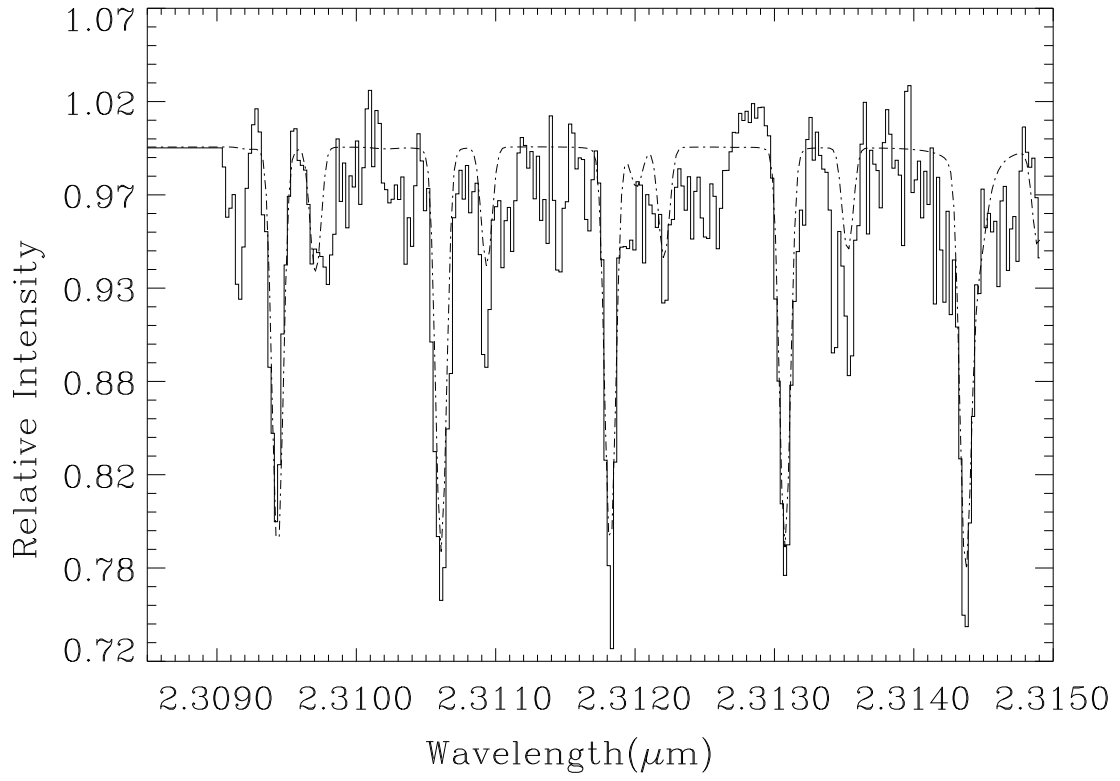


Fig. 2.— The solid histogram shows the observed CO lines of TW Hya. The dash-dotted curve shows the model spectrum produced by fitting the optical spectrum. No fitting was done to the CO lines.

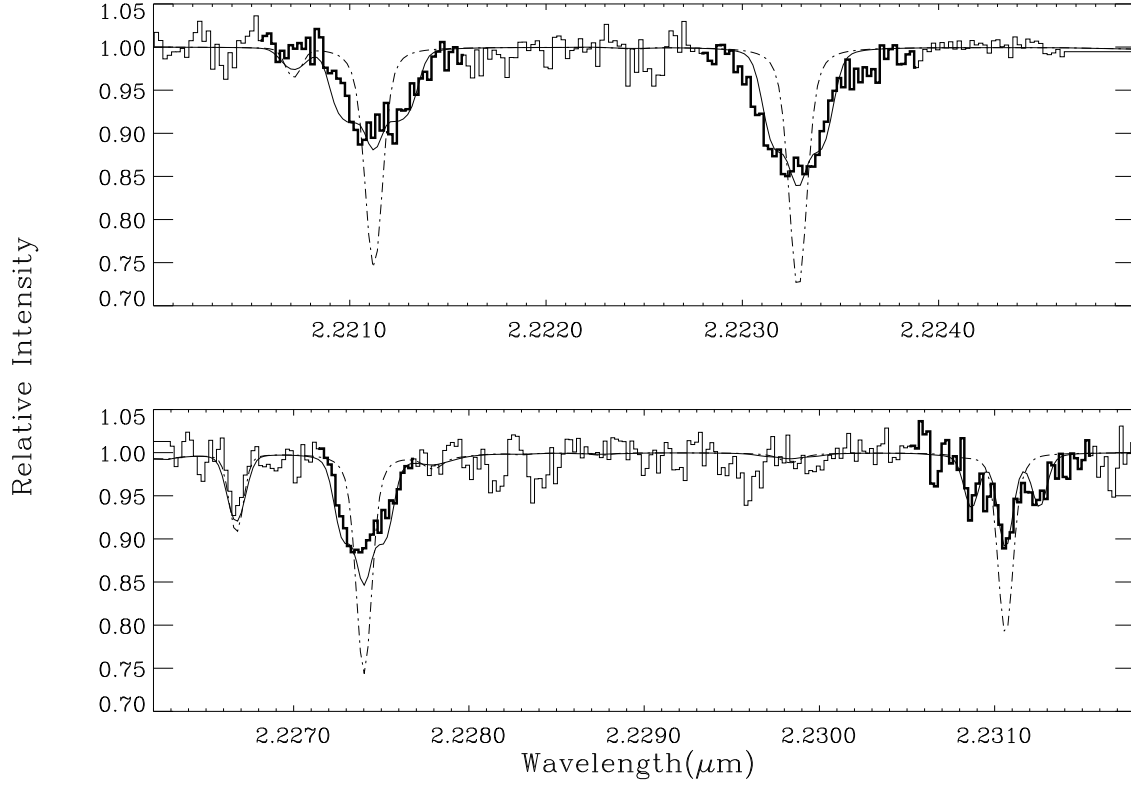


Fig. 3.— Best fit of infrared spectra using a single-component magnetic field model. Magnetically sensitive Ti I lines are fitted, where the bold regions indicate the portions of the spectrum actually used in the fit (histogram: data; dash-dotted line: fit without magnetic field; smooth solid line: fit with magnetic broadening).

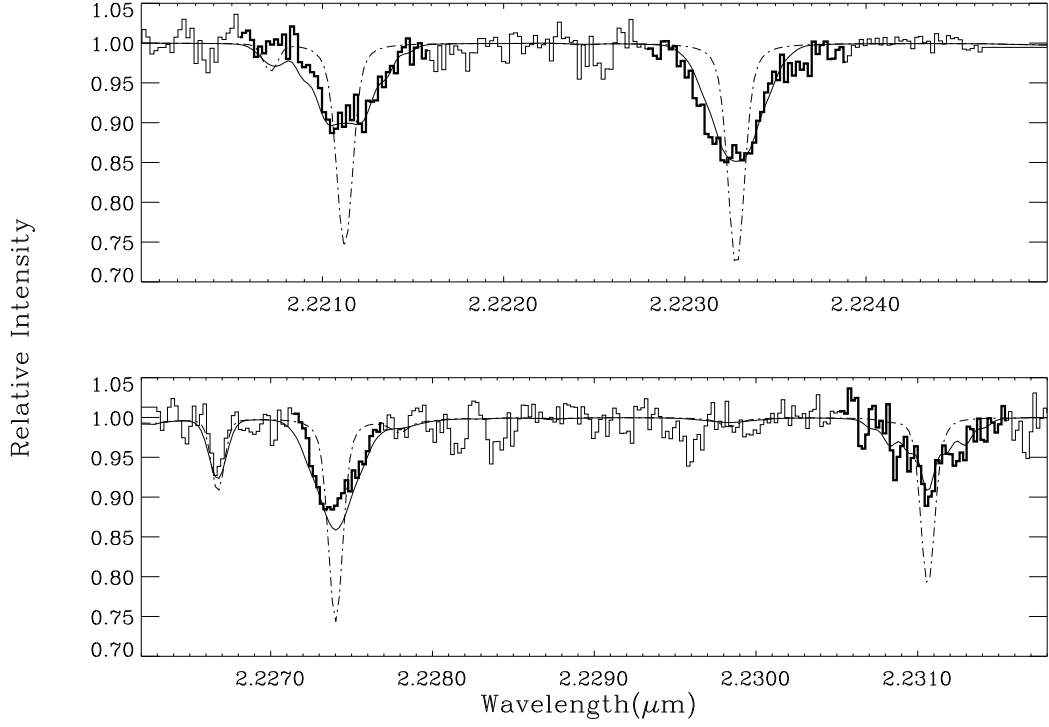


Fig. 4.— Best fit of infrared spectra using the multi-component magnetic field model M3. Magnetically sensitive Ti I lines are fitted with the regions actually used in the fit shown again in bold (histogram: data; dash-dotted line: fit without magnetic field; smooth solid line: fit with magnetic broadening).